

CHEMISTRY

A European Journal

A Journal of



Accepted Article

Title: A Crown-Shaped Ru-Substituted Arsenotungstate for Selective Oxidation of Sulfides with Hydrogen Peroxide

Authors: Jingyang Niu, Mengdan Han, Yanjun Niu, Rong Wan, Qiaofei Xu, Jingkun Lu, Pengtao Ma, Chao Zhang, and Jingping Wang

This manuscript has been accepted after peer review and appears as an Accepted Article online prior to editing, proofing, and formal publication of the final Version of Record (VoR). This work is currently citable by using the Digital Object Identifier (DOI) given below. The VoR will be published online in Early View as soon as possible and may be different to this Accepted Article as a result of editing. Readers should obtain the VoR from the journal website shown below when it is published to ensure accuracy of information. The authors are responsible for the content of this Accepted Article.

To be cited as: *Chem. Eur. J.* 10.1002/chem.201800748

Link to VoR: <http://dx.doi.org/10.1002/chem.201800748>

Supported by
ACES

WILEY-VCH

A Crown-Shaped Ru-Substituted Arsenotungstate for Selective Oxidation of Sulfides with Hydrogen Peroxide

Mengdan Han, Yanjun Niu, Rong Wan, Qiaofei Xu, Jingkun Lu, Pengtao Ma, Chao Zhang, Jingyang Niu* and Jingping Wang*[a]

Abstract: An acetate-bridged Ru-substituted arsenotungstate $[\text{H}_2\text{N}(\text{CH}_3)_2]_{14}[\text{As}_4\text{W}_{40}\text{O}_{140}(\text{Ru}_2(\text{CH}_3\text{COO}))_2] \cdot 22\text{H}_2\text{O}$ (**1**) has been synthesized and structurally characterized, in which four Ru atoms occupy all lacunary S2 sites of the crown-shaped polyanion $[\text{As}_4\text{W}_{40}\text{O}_{140}]^{28-}$ and each Ru atom is coordinated by one As atom and five $\mu_2\text{-O}$ atoms including four from S2 site and one from the acetate ligand. Notably, the novel coordination pattern of Ru atom in polyoxometalates (POMs) chemistry has been presented unprecedentedly, which is the formation of Ru–As bond with the length of 2.377(3)–2.387(3) Å. Particularly, **1** has exhibited high efficiency, splendid selectivity and good recyclability for the oxidation of sulfides with hydrogen peroxide (H_2O_2). It is worth mentioning that catalytic oxidation of various sulfides in the presence of **1** gave superior conversion and selectivity for sulfones in acetonitrile or sulfoxides in methanol.

Introduction

Polyoxometalates (POMs, predominantly polyoxotungstates and polyoxomolybdates) have triggered widespread attention over the past few decades not only because of their aesthetically fantastic structures, diverse compositions and the inimitable properties but also due to the potential applications in catalysis, electrochemistry, magnetism, and material science etc.^[1] Amongst the multitudinous polyoxometalate structural motifs, ruthenium(Ru)-substituted Keggin-type polyoxotungstates (RSKPs) endow POMs with unique catalytic properties due to the redox and catalytic properties of ruthenium.^[2] To our best knowledge, it has been proved that the RSKPs own wonderful catalysis towards the oxidation of various organic substrates, the reduction of carbon dioxide and water oxidation reaction.^[3] For instance, the mono-Ru-substituted silicotungstate $[\text{SiW}_{11}\text{O}_{39}\text{Ru}^{\text{III}}(\text{H}_2\text{O})]^{5-}$ first reported by Neumann could catalyze not only the oxidation of alkanes, alkenes and alcohols but also the photoreduction of carbon dioxide.^[4] Bonchio obtained a $\{\text{Ru}(\text{dmsO})\}^{2+}$ substituted phosphotungstate $[\text{PW}_{11}\text{O}_{39}\text{Ru}^{\text{II}}(\text{dmsO})]^{5-}$ which was documented as an efficient catalyst for the oxidation of cyclooctene.^[5a] Subsequently, Sadakane reported that $[\text{PW}_{11}\text{O}_{39}\text{Ru}^{\text{II}}(\text{dmsO})]^{5-}$ exhibited

catalytic activity towards water oxidation reaction.^[5b] Afterwards, the di-Ru-substituted POM $[\text{Ru}_2^{\text{III}}\text{Zn}_2(\text{H}_2\text{O})_2(\text{ZnW}_9\text{O}_{34})_2]^{14-}$ prepared by Shannon showed excellent electrocatalytic activity for oxygen generation.^[6] Therefore, the exploration of whole new types of RSKPs especially with attractive catalytic properties is scientifically significative and thus has been the subject of intensive synthetic efforts.

However, even after decades of research, the development of RSKPs chemistry is still in its infancy. To date, the known examples are mostly limited to the mono-/di-Ru-substituted species or their organo-ruthenium analogues, such as the mono-Ru-substituted derivatives $[\text{XW}_{11}\text{O}_{39}\text{Ru}(\text{H}_2\text{O})]^{5-/4-}$ ($\text{X} = \text{P}, \text{Si}, \text{Ge}$)^[4,7–10] and their dimethyl sulfoxide (dmsO) analogues $[\text{XW}_{11}\text{O}_{39}\text{Ru}(\text{dmsO})]^{5-/4-}$ ($\text{X} = \text{P}, \text{Si}, \text{Ge}$)^[5,8,10] $[\text{XW}_{11}\text{O}_{39}\text{Ru}(\text{dmsO})_3(\text{H}_2\text{O})]^{6-}$ ($\text{X} = \text{Si}^{\text{IV}}, \text{Ge}^{\text{IV}}$)^[11] the di-Ru-substituted derivatives $\{[(\text{WZnRu}_2^{\text{III}}(\text{OH})(\text{H}_2\text{O}))(\text{ZnW}_9\text{O}_{34})_2]^{11-}, [12]$ $[\text{Ru}_2^{\text{III}}\text{Zn}_2(\text{H}_2\text{O})_2(\text{ZnW}_9\text{O}_{34})_2]^{14-}, [6]$ the oxo-bridged derivatives $\{[\text{SiW}_{11}\text{O}_{39}\text{Ru}^{\text{IV/III}}_2\text{O}]^{11-}, [13]$ $\{[\text{PW}_{11}\text{O}_{39}]_2(\text{HO})\text{Ru}^{\text{IV}}\text{-O-Ru}^{\text{IV}}(\text{OH})\}^{10-}, [14]$ the ruthenium-nitrido derivatives $[\text{PW}_{11}\text{O}_{39}\text{Ru}^{\text{V}}\text{N}]^{4-}, [15]$ $[\gamma\text{-XW}_{10}\text{O}_{38}\{\text{RuN}\}_2]^{6-}$ ($\text{X} = \text{Si}, \text{Ge}$)^[16] and the arene-Ru derivatives $\{[\text{PW}_{11}\text{O}_{39}\{\text{Ru}(\text{arene})\}_2\{\text{WO}_2\}]^{8-}$ (arene = benzene, toluene, *p*-cymene, hexamethylbenzene)^[17] $[\text{XW}_{11}\text{O}_{39}\{\text{Ru}(\text{II})(\text{benzene})(\text{H}_2\text{O})\}]^{6-/5-}$ ($\text{X} = \text{P}, \text{Si}, \text{Ge}$)^[9] etc. Nevertheless, it is still a significant challenge to synthesize the multi-Ru-substituted polyoxotungstates.^[18–20] On the other hand, the majority of reported RSKPs are composed of WO_6 octahedra and XO_4 ($\text{X} = \text{P}^{\text{V}}, \text{Si}^{\text{IV}}, \text{Ge}^{\text{IV}}$, etc.) tetrahedra. In comparison, the introduction of trigonal pyramidal XO_3 ($\text{X} = \text{As}^{\text{III}}, \text{Sb}^{\text{III}}, \text{Bi}^{\text{III}}, \text{Se}^{\text{VI}}, \text{Te}^{\text{VI}}$) groups into Ru-substituted polyoxotungstates remains largely unexplored. Up to now, only a handful of RSKPs based on trigonal pyramidal XO_3 ($\text{X} = \text{As}^{\text{III}}, \text{Sb}^{\text{III}}, \text{Bi}^{\text{III}}, \text{Se}^{\text{VI}}, \text{Te}^{\text{VI}}$) groups were addressed.^[20–23] When search for a new entry into RSKPs chemistry, we first utilized the self-assembly strategy of sodium tungstate, heteroatom ingredients such as sodium arsenite to react with ruthenium ions aimed at discovering novel RSKPs for the following reasons: a) The self-assembly strategy is an effective method to construct POMs with diverse structures and compositions. b) The stereochemically active lone pair on the As^{III} atom always precludes the formation of closed Keggin units, which makes it possible that ruthenium ions can incorporate into the lacunary sites, or more likely, integrate in situ generated fragments together into large architectures.

Herein, we present a new acetate-bridged Ru-substituted arsenotungstate $[\text{H}_2\text{N}(\text{CH}_3)_2]_{14}[\text{As}_4\text{W}_{40}\text{O}_{140}(\text{Ru}_2(\text{CH}_3\text{COO}))_2] \cdot 22\text{H}_2\text{O}$ (**1**), which was obtained successfully by the reaction of $\text{Na}_2\text{WO}_4 \cdot 2\text{H}_2\text{O}$, NaAsO_2 and RuCl_3 in the presence of dimethylamine hydrochloride in sodium acetate buffer solution. The excellent catalytic activity of **1** was observed towards the selective oxidation of sulfides with hydrogen peroxide (H_2O_2). High selectivity and good conversions of sulfones or sulfoxides could be obtained when the catalytic process was performed in corresponding solvents (acetonitrile or methanol, respectively). The results of recycling experiments implied that there were no

[a] M. Han, Y. Niu, R. Wan, Q. Xu, J. Lu, Dr. P. Ma, Dr. C. Zhang, Prof. J. Niu, Prof. J. Wang
Key Laboratory of Polyoxometalate Chemistry of Henan Province
Institute of Molecular and Crystal Engineering
College of Chemistry and Chemical Engineering
Henan University, Kaifeng, Henan 475004 (P. R. China)
Fax: (+ 86)371-238-868-76
E-mail: jyniu@henu.edu.cn
jpwang@henu.edu.cn

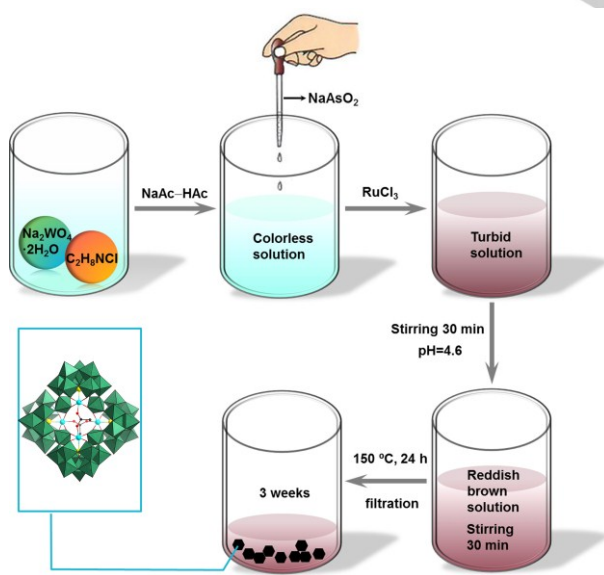
Supporting information for this article is given via a link at the end of the document.

obvious changes in conversion and selectivity for the oxidation of methyl phenyl sulfide to methyl phenyl sulfone in acetonitrile across five runs, which showed the superior recyclability of **1**.

Results and Discussion

Synthesis

The design and synthesis of RSKPs remain a great challenge because of the intricacies in their synthetic mechanism. As a result, it is quite difficult to search appropriate reaction conditions that can allow access to novel RSKPs. With unremitting efforts, we have now succeeded in preparing a new crown-shaped Ru-substituted arsenotungstate $[\text{H}_2\text{N}(\text{CH}_3)_2]_{14}[\text{As}_4\text{W}_{40}\text{O}_{140}\{\text{Ru}_2(\text{CH}_3\text{COO})\}_2] \cdot 22\text{H}_2\text{O}$ (**1**) by reaction of $\text{Na}_2\text{WO}_4 \cdot 2\text{H}_2\text{O}$, NaAsO_2 and RuCl_3 with a molar ratio of 7.7:1.1:1.0 in the sodium acetate buffer solution (0.5 mol L^{-1} , $\text{pH} = 4.3$) in the presence of dimethylamine hydrochloride (Scheme 1). Importantly, the sodium acetate buffer solution, as a reaction medium, plays a vital role in the construction of **1**. It not only supplies a mild environment for Ru ions, preventing them from hydrolyzing, but also provides the bidentate ligands CH_3COO^- that can coordinate to Ru ions. Besides, when the pH value of the solution was adjusted to about 4.6, the quality of the crystals was best. Another essential aspect in the formation of **1** is the counter cations. Initially, we selected Na^+ , K^+ , Rb^+ and Cs^+ as counter cations, however, no desired crystals were obtained. In our subsequent exploration, dimethylamine hydrochloride was introduced into our reaction system. We found that the solubility of Ru ions was increased in the presence of dimethylamine hydrochloride, which facilitates Ru ions incorporated into in situ generated arsenotungstate fragments, giving birth to the title compound.



Scheme 1. The schematic synthetic process of compound **1**.

Crystal Structure

Single-crystal structural analysis reveals that compound **1** crystallizes in the monoclinic space group $P2_1/c$ and contains a crown-shaped Ru-substituted arsenotungstate $[\text{As}_4\text{W}_{40}\text{O}_{140}\{\text{Ru}_2(\text{CH}_3\text{COO})\}_2]^{14-}$ (**1a**), fourteen monoprotonated $[\text{H}_2\text{N}(\text{CH}_3)_2]^+$ counter cations and twenty-two lattice water molecules. The polyanion $[\text{As}_4\text{W}_{40}\text{O}_{140}\{\text{Ru}_2(\text{CH}_3\text{COO})\}_2]^{14-}$ comprises a cyclic unit $[\text{As}_4\text{W}_{40}\text{O}_{140}]^{28-}$ ($\{\text{As}_4\text{W}_{40}\}$) with two $[\text{Ru}_2(\text{CH}_3\text{COO})]^{7+}$ ($\{\text{Ru}_2(\text{CH}_3\text{COO})\}$) segments embedded in its cavities (Figure 1c and Figure S1). The $\{\text{As}_4\text{W}_{40}\}$ unit (Figure 1b) is constructed from four trivacant $[\text{B}-\alpha\text{-AsW}_9\text{O}_{33}]^{9-}$ ($\{\text{AsW}_9\}$) fragments (Figure 1a) joined together by four additional WO_6 octahedra, and is already confirmed as a multi-vacant cryptate which contains four coordinative sites S2 and a central cryptate site S1 (Figure S2).^[24] Each WO_6 octahedron links two adjacent $\{\text{AsW}_9\}$ fragments by two $\mu_2\text{-O}$ atoms. The remaining oxygen atoms of each WO_6 octahedron together with two oxygen atoms of each $\{\text{AsW}_9\}$ fragment define the S2 sites and the eight remaining oxygen atoms of four WO_6 octahedra define the central site S1. In the polyanion **1a**, all the lacunary S2 sites of the $\{\text{As}_4\text{W}_{40}\}$ are occupied by four Ru atoms whereas the central site S1 remains vacant. A bidentate acetate ligand connects two diametrically opposed Ru atoms in a $(\mu_2\text{-}\eta^1\text{:}\eta^1)$ fashion, giving rise to a $\{\text{Ru}_2(\text{CH}_3\text{COO})\}$ segment with a $\text{Ru}\cdots\text{Ru}$ distance of $5.9147(3) \text{ \AA}$ (Figure S3). As far as we know, such a crown-shaped acetate-bridged Ru-substituted arsenotungstate is a first report that supports the structural novelty of this rare compound. Interestingly, there are two crystallographically independent Ru atoms (Ru1 and Ru2) in the asymmetric unit which are hexa-coordinated and adopt distorted octahedral geometries (Figure 2a-b). Both Ru atoms are defined by two $\mu_2\text{-O}$ atoms from the $\{\text{AsW}_9\}$ fragment $[\text{Ru}-\text{O}, 1.979(18)\text{--}2.067(19) \text{ \AA}]$, two $\mu_2\text{-O}$ atoms from two WO_6 octahedra $[\text{Ru}-\text{O}, 1.995(18)\text{--}2.022(17) \text{ \AA}]$, one $\mu_2\text{-O}$ atom from the $\{\text{CH}_3\text{COO}\}$ group $[\text{Ru}-\text{O}_{\text{COO}}, 2.105(18)\text{--}$

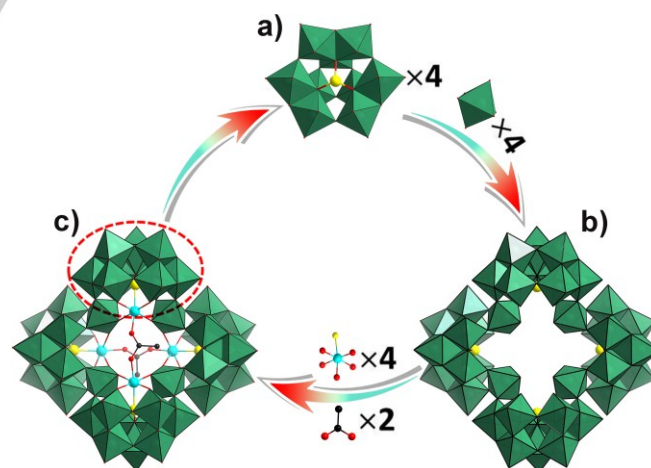


Figure 1. a) Ball-and-stick/polyhedral representation of the $[\text{B}-\alpha\text{-AsW}_9\text{O}_{33}]^{9-}$ fragment in **1a**. b) Ball-and-stick/polyhedral representation of the cryptate $[\text{As}_4\text{W}_{40}\text{O}_{140}]^{28-}$. c) Ball-and-stick/polyhedral representation of the polyanion **1a**. Color code: WO_6 octahedra, sea green; ruthenium, turquoise; arsenic, yellow; oxygen, red; carbon, black, all the hydrogen atoms are omitted for clarity.

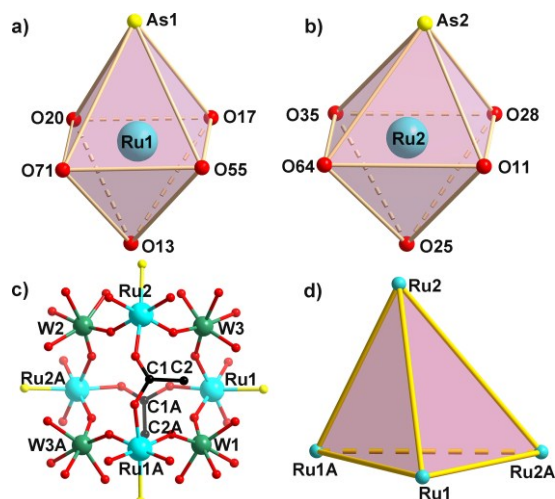


Figure 2. a) The coordination environment of Ru1 ion. b) The coordination environment of Ru2 ion. c) The octa-nuclear heterometallic $[\text{Ru}_4\text{W}_4\text{O}_8(\text{CH}_3\text{COO})_2]^{22+}$ core in **1a**. d) The trigonal pyramid geometry of tetra-nuclear Ru cluster. Atoms with A in their labels are symmetrically generated. A: 2-x, y, 1.5-z.

2.11(2) Å], and one As atom from the $\{\text{AsW}_9\}$ fragment [Ru–As, 2.377(3)–2.387(3) Å]. Herein, it is worth mentioning that the Ru–As bond in **1a** has been observed for the first time in POMs chemistry. Remarkably, irrespective of the $\{\text{AsW}_9\}$ fragments, the remanent eight metals including four Ru and four W cations are interconnected by eight $\mu_2\text{-O}$ and two acetate bridges, resulting in an octa-nuclear heterometallic core $[\text{Ru}_4\text{W}_4\text{O}_8(\text{CH}_3\text{COO})_2]^{22+}$ (Figure 2c), where four Ru cations reside in a distorted tetrahedron (Figure 2d).

It should be pointed out that the polyanion **1a** somewhat resembles to $[(\text{H}_2\text{O})_{10}(\text{Ce}^{\text{III}}\text{OH})_2(\text{B-}\alpha\text{-AsW}_9\text{O}_{33})_4(\text{WO}_2)_4]^{18-}$ previously reported by Pope et al, in which four S2 sites are occupied by four Ce atoms (Figure S4a).^[25] Nevertheless, there are also obvious differences between them apart from containing the same $\{\text{As}_4\text{W}_{40}\}$ unit: (a) the former is an acetate acid containing organic-inorganic hybrid cluster, while the latter is a pure inorganic cluster; (b) the former consists of a tetra-ruthenium-containing heterometallic core $[\text{Ru}_4\text{W}_4\text{O}_8(\text{CH}_3\text{COO})_2]^{22+}$ (Figure 2c) while the latter includes a tetra-cerium-containing bimetal-oxide core $[\text{Ce}_4\text{W}_4\text{O}_8(\text{OH})_2(\text{H}_2\text{O})_{10}]^{18+}$ (Figure S4b); (c) in the former, four Ru atoms are hexa-coordinated and defined by one As atom and five $\mu_2\text{-O}$ atoms, on the contrary, four Ce atoms in the latter are all eight-coordinated and defined by five $\mu_2\text{-O}$ atoms and three water molecules; (d) in the former, two pairs of opposite Ru atoms are all linked together by a bidentate acetate bridge; whereas in the latter, the opposite two of four Ce atoms are joined together by a $\mu_2\text{-O}$ bridge; (e) the former was obtained from the WO_4^{2-} , AsO_2^- and Ru^{3+} via the self-assembly strategy whereas the latter was obtained from the cryptate precursor $[\text{As}_4\text{W}_{40}\text{O}_{140}]^{28-}$.

From another perspective, the polyanion **1a** can be perceived as follows: two $\{\text{AsW}_9\}$ fragments (Figure 3a) are joined together by a $\{\text{Ru}_2(\text{CH}_3\text{COO})\}$ segment (Figure 3b), forming a dimeric

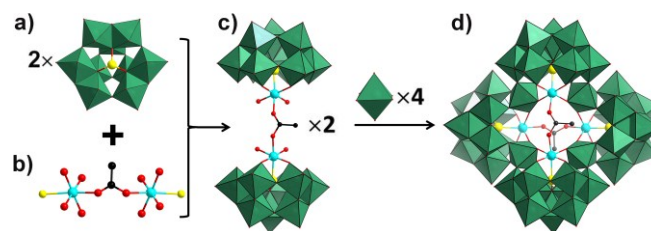


Figure 3. a) The $[\text{B-}\alpha\text{-AsW}_9\text{O}_{33}]^{9-}$ fragment. b) The $\{\text{Ru}_2(\text{CH}_3\text{COO})\}$ segment. c) The dimeric mono-Ru-substituted arsenotungstates $[(\text{B-}\alpha\text{-AsW}_9\text{O}_{33})_2\text{Ru}_2(\text{CH}_3\text{COO})]^{11-}$. d) The polyanion **1a**.

mono-Ru-substituted arsenotungstate $[(\text{B-}\alpha\text{-AsW}_9\text{O}_{33})_2\text{Ru}_2(\text{CH}_3\text{COO})]^{11-}$ (Figure 3c). Two $[(\text{B-}\alpha\text{-AsW}_9\text{O}_{33})_2\text{Ru}_2(\text{CH}_3\text{COO})]^{11-}$ subunits in a vertical cross arrangement are linked by four additional WO_6 octahedra, resulting in a cyclic tetrameric motif (Figure 3d). Notably, the linking mode of the acetate ligand in $[(\text{B-}\alpha\text{-AsW}_9\text{O}_{33})_2\text{Ru}_2(\text{CH}_3\text{COO})]^{11-}$ subunits is different from that of in acetate-bridged mono-lanthanide substituted polyoxotungstates $[(\text{La}(\text{CH}_3\text{COO})(\text{H}_2\text{O})_2(\alpha\text{-P}_2\text{W}_{17}\text{O}_{61}))_2]^{16-}$,^[26] $[(\alpha\text{-SiW}_{11}\text{O}_{39})\text{Ln}(\mu\text{-COOCH}_3)(\text{H}_2\text{O})_2]^{12-}$ (Ln = Gd^{III} and Yb^{III})^[27] and $[(\alpha\text{-PW}_{11}\text{O}_{39})\text{Ln}(\text{H}_2\text{O})(\eta^2, \mu\text{-1,1})\text{-CH}_3\text{COO}]_2^{10-}$ (Ln = Sm^{III}, Eu^{III}, Gd^{III}, Tb^{III}, Ho^{III} and Er^{III})^[28] where two Ln atoms are doubly bridged by two acetate molecules in a $(\eta^2, \mu\text{-1,1})$ fashion (Figure S5).

Bond valence sums (BVS)^[29] calculated for the two crystallographically independent Ru atoms lie between 3.78 and 3.92, indicating that Ru atoms are +IV valence states (Table S1). Additionally, the oxidation of Ru^{III} in reaction solution to yield a Ru^{IV}-containing POM has been reported.^[30] The BVS values for W and As atoms are 6.04–6.81 and 2.43–2.56, respectively (Table S2 and Table S3), indicating that all the W and As are in the +6 and +3 oxidation states, respectively. In addition, the BVS values for the oxygen atoms including the oxygen atoms from $\{\text{CH}_3\text{COO}\}$ groups are in the range of 1.68–2.20 (Table S4), indicating that all the oxygen atoms are deprotonated.

IR spectrum

The IR spectrum of **1** shows the characteristic vibrations in the region of 1000–650 cm^{-1} . The prominent peak at 962 cm^{-1} is attributed to the terminal W-O_t vibrations. Peaks at 891 cm^{-1} , 749 cm^{-1} are derived from the two types of W-O-W stretching vibrations and the peak at 705 cm^{-1} is attributed to the W-O(As) vibration.^[31] The strong peak at 834 cm^{-1} is attributed to As-O vibration. Additionally, the broad peaks at 3435 cm^{-1} and 1623 cm^{-1} are assigned to the stretching and bending modes of lattice water molecules.^[32] The weak bands at 3120 and 2926 cm^{-1} are derived from the N–H and C–H stretching vibrations,^[33] illustrating the existence of dimethylamine hydrochloride. In addition, peaks appearing at 1623 cm^{-1} and 1464 cm^{-1} are attributed to the asymmetric and symmetric stretching vibrations of the CH_3COO^- ligands, respectively, with the former band overlapping with the bending vibration of the lattice water (Figure S6).

Powder X-ray diffraction

As shown in Figure S7, the powder X-ray diffraction peaks are in good agreement with the simulated peaks originated from single-crystal X-ray diffraction, indicating the good phase purity for the targeted samples. The differences in intensity between the experimental and simulated patterns may be attributed to the variation in preferred orientation of the powder sample in the process of collection of the experimental PXRD.

UV-vis spectra

The UV-vis spectrum of **1** in the low concentrated aqueous solution (1.0×10^{-6} mol L⁻¹) displays two characteristic peaks at 200 nm and 250 nm in the range of 400–190 nm (Figure 4a). The higher energy absorption at 200 nm can be ascribed to the $\pi\pi$ - $d\pi$ charge-transfer transition of the O_l-W bands, whereas the lower at 250 nm can be assigned to the $\pi\pi$ - $d\pi$ charge-transfer transition of the O_{b,c}-W bands.^[34] In the visible region, a broad peak at around 478 nm is observable in more concentrated solution (1.0×10^{-4} mol L⁻¹) (Figure 4b), which can be ascribed to O→Ru charge transfer.^[12,35]

The pH-varying absorption spectra of **1** in the visible region were also investigated as POMs are sensitive to the pH value. Diluted HCl solution and NaOH solution were used to adjust the pH values in the acidic direction and in the alkaline direction, respectively. The initial pH value of **1** in aqueous solution was 5.8. As shown in Figure 4c and 4d, as the pH value decreased, the absorbance band at around 478 nm became weaker and weaker. In contrast, the absorbance band is gradually red-shifted at pH higher than 9.3. Besides, the on-going spectroscopic measurements were also conducted in the aqueous system (Figure S10). And **1** can stably exist in the aqueous system within 1 hour at ambient temperature.

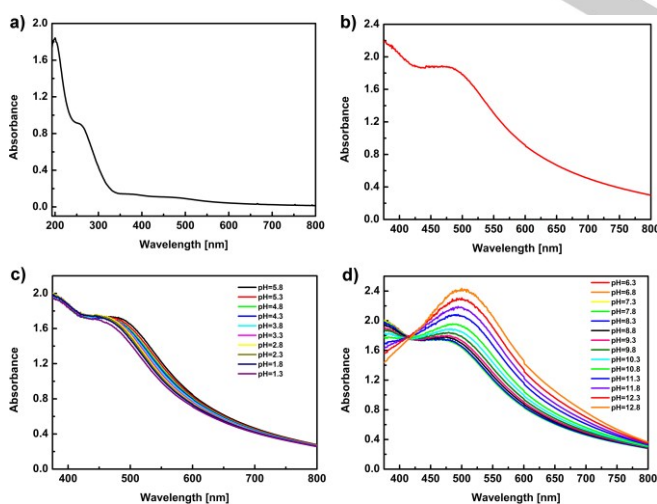


Figure 4. The UV-vis spectra of **1** a) in the low concentrated solution (1.0×10^{-6} mol L⁻¹). b) in more concentrated solution (1.0×10^{-4} mol L⁻¹). c) and d) at different pH values.

ESI-MS study

The negative-ion electrospray-ionization mass spectrometry (ESI-MS) was performed to study the cluster species in solution. Single-crystalline samples of **1** were dissolved in a mixed solvent (V(H₂O)/V(CH₃CN) = 9:1, 4.5 mL H₂O, CH₃CN 0.5 mL). As shown in Figure 5a, the ESI-MS spectrum displays three dominant peaks corresponding to the intact cluster. These peaks were assigned to charge values of 7, 6 and 5 at m/z of 1505.68 [(H₂N(CH₃)₂)₁H₆As₄W₄₀Ru₄O₁₄₀(CH₃COO)₂(H₂O)₄]⁷⁻ (simulated 1505.69), 1756.80 [(H₂N(CH₃)₂)₁H₇As₄W₄₀Ru₄O₁₄₀(CH₃COO)₂(H₂O)₄]⁶⁻ (simulated 1756.81) and 2131.79 [(H₂N(CH₃)₂)₂H₇As₄W₄₀Ru₄O₁₄₀(CH₃COO)₂(H₂O)₈]⁵⁻ (simulated 2131.79), respectively (Figure 5b-d). Furthermore, the simulated isotopic pattern at around m/z 2137.18 [(H₂N(CH₃)₂)₁H₈As₄W₄₀Ru₄O₁₄₀(CH₃COO)₂(H₂O)₁₂]⁵⁻ is provided in the Supporting Information (Figure S14).

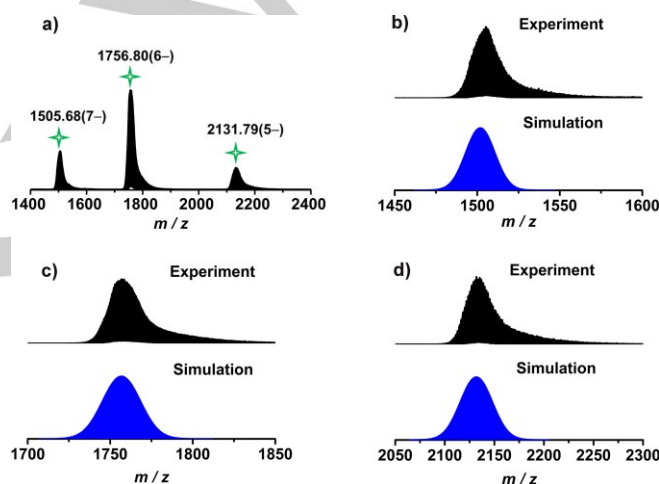


Figure 5. a) The ESI-MS spectrum corresponding to the intact cluster (zoom in of the peaks at around 1505.68, 1756.80, 2131.79 were provided in supporting information, Figure S11-S13). b), c) and d) The simulated (blue) and experimental (black) patterns at around m/z 1505.68, 1756.80, 2131.79.

Catalysis

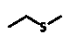
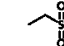
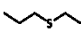
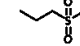
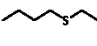
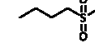
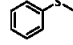
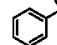
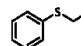
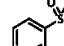
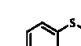
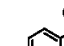
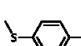
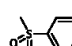
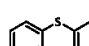
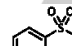
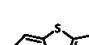
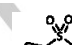


The selective oxidation of sulfides is a meaningful and important process as the corresponding sulfones and sulfoxides are extensively used in the synthesis of biological and pharmaceutical compounds,^[36] fine chemicals,^[37] and as ligands in asymmetric catalysis.^[38] Here, catalytic reactions were performed with hydrogen peroxide (H₂O₂) to investigate the catalytic efficiency of **1** towards the heterogeneous oxidation of sulfides. Initially, methyl phenyl sulfide (MPS) was used as the benchmark substrate to study the catalytic oxidation of sulfides in the presence of **1** in acetonitrile, which showed 99% conversion and 53% selectivity for methyl phenyl sulfone at 50°C (Table S5, entry 5). In the subsequent catalytic reactions, selectivity for methyl phenyl sulfone was promoted with increasing the dosage of H₂O₂ and reached 100% until 2.5 mmol H₂O₂ was used under otherwise identical conditions (Table 1,

Table 1. Oxidation of methyl phenyl sulfide using **1** with H₂O₂ in acetonitrile^[a]

Entry	Catalyst (μmol)	H ₂ O ₂ (mmol)	Temp. (°C)	Time (min)	Conv. ^[b] (%)	Sel. ^[c] (%)
1	1.6	2.5	25	60	93	63
2	0.8	2.5	50	60	99	77
3	1.6	2.0	50	60	99	79
4	1.6	2.5	50	30	96	67
5	1.6	2.5	50	60	100	100

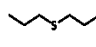
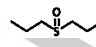
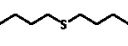
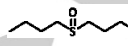
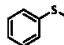
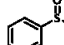
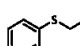
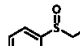
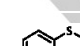
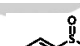

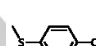
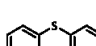
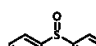
[a] Reaction conditions: substrate (1 mmol), 30% H₂O₂ (2.0 mmol, 2.5 mmol), catalyst (0.8 μmol, 1.6 μmol), acetonitrile (3 mL). [b] Conversions were determined by GC-FID using an internal standard technique and are based on substrates. [c] Selectivity for sulfone. The products were identified by GC-MS.

Table 2. Selective oxidation of sulfides to sulfones using **1** with H₂O₂ in acetonitrile^[a]

Entry	Substrate	Product	Time (min)	Conv. ^[b] (%)	Sel. ^[c] (%)
1			30	100	100
2			50	100	100
3			60	100	100
4			60	100	100
5			60	100	100
6			60	100	100
7			60	100	100
8			90	99	97
9			120	69	100
10			180	52	98.5

[a] Reaction conditions: substrate (1 mmol), 30% H₂O₂ (2.5 mmol), catalyst (1.6 μmol), acetonitrile (3 mL), 50 °C. [b] Conversions were determined by GC-FID using an internal standard technique and are based on substrates. [c] Selectivity for sulfones. The products were identified by GC-MS.

Table 3. Selective oxidation of sulfides to sulfoxides using **1** with H₂O₂ in methanol^[a]

Entry	Substrate	Product	Time (min)	Conv. ^[b] (%)	Sel. ^[c] (%)
1			50	98.3	88.3
2			50	97.7	89
3			60	97.4	87
4			60	97	85
5			60	98	84.3
6			60	96.6	79
7			120	48	96

[a] Reaction conditions: substrate (1 mmol), 30% H₂O₂ (2.5 mmol), catalyst (1.6 μmol), methanol (3 mL), 50 °C. [b] Conversions were determined by GC-FID using an internal standard technique and are based on substrates. [c] Selectivity for sulfoxides. The products were identified by GC-MS.

entries 3 and 5). The results indicated that 2.5 mmol H₂O₂ was the optimum amount under these conditions. In addition, the sulfone selectivity decreased dramatically when the loading of catalyst was reduced to 0.8 μmol (Table 1, entry 2). Furthermore, a series of experiments were also carried out to explore the effects of the reaction time and temperature on the conversion and selectivity of MPS. The corresponding sulfoxide and sulfone products were verified by GC-MS (Figure S17-S18). The results implied that the reaction time and temperature also played crucial role in the conversion and selectivity of MPS (Table 1, entries 1 and 4). On the basis of the above results, it is obvious that the optimum temperature and reaction time are 50 °C and 60 min, respectively. As control experiments, the blank experiment without **1** was performed in acetonitrile, with only 38% conversion and 54% selectivity observed (Table S5, entry 1). Besides, catalytic activity of Na₂WO₄·2H₂O, RuCl₃ and the mixture of these two materials for the oxidation of MPS were also independently investigated for comparison. As presented in TableS5, the catalyst RuCl₃ exhibited low conversion for the reaction (Table S5, entry 2) while Na₂WO₄·2H₂O and the mixture of Na₂WO₄·2H₂O and RuCl₃ gave 89% and 90% conversion, respectively (Table S5, entries 3 and 4). However, these two synthetic materials were homogeneous catalysts in our reaction system that couldn't be separated and reused. Therefore, catalyst **1**, on the whole, was superior to the synthetic materials, and these results indicated that the main catalytic center is the POM unit. Under optimal conditions (1.6 μmol catalyst, 1 mmol substrate and 2.5 mmol 30% H₂O₂ in 3 mL acetonitrile at 50 °C), MPS was converted to the expected sulfone with 100% conversion and selectivity (Table 1, entry 5). Encouraged by the

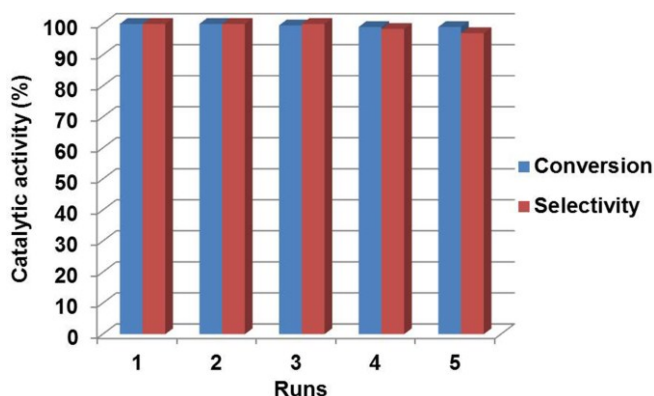


Figure 6. Recycling of compound 1 catalytic system for the oxidation of methyl phenyl sulfides to methyl phenyl sulfone.

catalytic activity of **1** towards the oxidation of MPS in acetonitrile, a scope of experiments were also carried out under optimal conditions to test the catalytic universality of **1**, which was presented detailedly in Table 2. Gratifyingly, dialkyl sulfides (Table 2, entries 1–3) and some alkylaryl sulfides such as ethyl phenyl sulfide, 4-methylthioanisole, 4-methoxythioanisole tested (Table 2, entries 5–7) were entirely converted with 100% selectivity for the corresponding sulfones. However, for diphenyl thioether, longer reaction time (90 min) was required to achieve comparable conversion and selectivity, which might be ascribed to the low electron density of the sulfur atom in this substrate (Table 2, entry 8). Oxidation of refractory sulfur-containing compounds including dibenzothiophene (DBT) and benzothiophene (BT) were also studied, but reluctant conversions were obtained (Table 2, entries 9 and 10). Notably, the corresponding reactions which followed the optimum conditions but performed in methanol gave sulfoxides as major product with high conversions (96.6%–98.3%) and good selectivity (79–89%) with the exception of diphenyl thioether which reached 48% conversion and 96% selectivity for its sulfoxide after 120 min (Table 3). In this regard, previous reports have reported that the solvent has a significant influence on the selectivity of sulfoxidation.^[39]

The hot filtration experiment was conducted under optimal conditions. **1** was removed at a reaction time of 15 min, and the reaction was allowed to proceed with the filtrate. Only a very small increase in conversion of MPS was observed, suggesting that this oxidation process is heterogeneous (Figure S19).^[40] Besides, recycle reactions on the oxidation of MPS were performed in acetonitrile to evaluate the recyclability of the catalyst. After the oxidation reaction, the catalyst was separated from the solvent/oxidant/substrate system by filtration, washed with acetonitrile, dried and reused for the next run. The recycling experiments showed that **1** could be reused five runs without distinguishable decrease in conversion and sulfone selectivity (Figure 6).

Although noticeable increase of the intensity of the bonds at 834 cm^{-1} and 749 cm^{-1} are observable (Figure S20a), the IR spectra of the recovered catalysts are almost identical to that of fresh catalyst, all of which display the typical bands of the

framework structure (Figure S20b). According to the ESI-MS spectrum of the recovered catalyst after fifth-run, the skeleton of the structure was still retained (Figure S21).

Conclusions

In summary, we have reported a crown-shaped organic-inorganic hybrid Ru-substituted arsenotungstate, to the best of our knowledge, which represents the first example of acetate-bridged Ru-substituted POMs and the Ru-As bond in **1** has been reported for the first time in POMs chemistry. Importantly, **1** exhibits significant catalytic activity for the selective oxidation of sulfides with hydrogen peroxide under mild conditions. Catalytic reactions conducted in acetonitrile gave sulfone as the major product with high selectivity while high sulfoxide selectivity with excellent yields was obtained in methanol. In subsequent work, continuing efforts will be devoted to constructing novel Ru-substituted POMs with intriguing architectures and excellent catalytic properties by adjusting different reaction components such as different heteroatoms and carboxylates. We believe that this work will enrich the structural diversity of POMs and stimulate the development of POM chemistry.

Experimental Section

Material and physical measurements

IR spectra were collected on a Bruker VERTEX 70 IR spectrometer using KBr pellets in the range of 4000–400 cm^{-1} . UV-vis absorption spectra were obtained on a U-8100 spectrometer at room temperature. Thermogravimetric analysis (TGA) was performed on a NETZSCH STA 449F5/QMS403D instrument under a nitrogen gas atmosphere with a heating rate of 10 $^{\circ}\text{C min}^{-1}$ from 30 to 900 $^{\circ}\text{C}$. Elemental analyses of C, H, and N were obtained on an Elementar Vario EL cube CHNS analyzer. Inductively coupled plasma (ICP) spectra were conducted on a Perkin-Elmer Optima 2000 ICP-OES. Powder X-ray diffraction (PXRD) were collected on Bruker D8 Advance instrument with Cu K α radiation ($\lambda = 1.5418 \text{ \AA}$) in the angular range $2\theta = 5\text{--}50^{\circ}$ at 293 K. ESI-MS spectrometry was performed on an ABSCIEX Triple TOF 4600 mass spectrometer. The ESI-MS spectrum of the catalyst after fifth-run was obtained on a Q EXACTIVE mass spectrometry. The ^1H NMR (400 MHz) and ^{13}C NMR (101MHz) spectra were detected on a Bruker AVANCE III HD spectrometer with TMS as the internal standard. A freshly cleaned glassy carbon disk electrode (3 mm diameter) was used as a working electrode, a platinum wire served as the counter electrode and an Ag/AgCl electrode as the reference electrode.

Preparation of $[\text{H}_2\text{N}(\text{CH}_3)_2]_{14}[\text{As}_4\text{W}_{40}\text{O}_{140}(\text{Ru}_2(\text{CH}_3\text{COO}))_2] \cdot 22\text{H}_2\text{O}$: $\text{Na}_2\text{WO}_4 \cdot 2\text{H}_2\text{O}$ (2.210 g, 6.700 mmol) and dimethylamine hydrochloride (0.510 g, 6.255 mmol) were dissolved in 20 mL sodium acetate buffer solution (0.5 mol L^{-1} , pH = 4.3) with stirring. NaAsO_2 (1 mol L^{-1} , 1 mL) was dropwise added to the solution. Then, RuCl_3 (0.180 g, 0.868 mmol) was subsequently added into the reaction mixture. Immediately, lots of precipitate was formed and the solution became turbid. After stirring for 30 min, the precipitate dissolved completely and the pH of the solution was adjusted to about 4.6 with glacial acetic acid. On further stirring for another 30 min, the reddish brown solution was sealed in a Teflon-lined autoclave and heated at 150 $^{\circ}\text{C}$ for 24 h. After cooling to room

Table 4. Crystallographic data for **1**.

Empirical formula	C ₃₂ H ₁₆₂ N ₁₄ O ₁₆₆ As ₄ Ru ₄ W ₄₀
Formula weight	11457.19
Crystal system	Monoclinic
Space group	<i>P</i> 2/ <i>c</i>
<i>a</i> (Å)	35.371(3)
<i>b</i> (Å)	20.1245(17)
<i>c</i> (Å)	30.087(3)
β °	109.104(2)
<i>V</i> (Å ³)	20237(3)
<i>Z</i>	4
<i>D</i> _{calcd} (g cm ⁻³)	3.461
μ (mm ⁻¹)	23.648
<i>F</i> (000)	18088.0
Crystal size (mm ³)	0.28 × 0.16 × 0.14
Index ranges	-42 ≤ <i>h</i> ≤ 41; -21 ≤ <i>k</i> ≤ 24; -35 ≤ <i>l</i> ≤ 35
Reflections collected	103686
Independent reflections	35939
Data/restraints/parameters	35939/2/1057
<i>R</i> _{int}	0.1077
GOF on <i>F</i> ²	1.015
<i>R</i> ₁ , <i>wR</i> ₂ [<i>I</i> > 2σ(<i>I</i>)]	<i>R</i> ₁ = 0.0694, <i>wR</i> ₂ = 0.1509
<i>R</i> ₁ , <i>wR</i> ₂ [all data]	<i>R</i> ₁ = 0.1340, <i>wR</i> ₂ = 0.1823

temperature, the reaction solution was filtered. Slow evaporation of the filtrate at room temperature resulted in the black hexagonal crystals that were suitable for single-crystal X-ray diffraction in about three weeks. Yield: 0.02 g (0.8% based on RuCl₃); IR (KBr, pellet): ν 3435, 3120, 2926, 2853, 1623, 1516, 1464, 962, 891, 834, 782, 749, 705, 618 cm⁻¹; elemental analysis calcd (%) for [H₂N(CH₃)₂]₁₄[As₄W₄₀O₁₄₀{Ru₂(CH₃COO)}₂·22H₂O: C 3.35, H 1.43, N 1.71, As 2.62, Ru 3.53, W 64.18; found: C 3.51, H 1.57, N 1.70, As 2.31, Ru 3.17, W 63.10.

X-ray crystallography: A black hexagonal crystal of **1** was selected under an optical microscope and airproofed in a capillary tube as the crystal was easy to weathering. Single-crystal X-ray diffraction intensity data for **1** were obtained on a Bruker APEX-II CCD diffractometer with graphite-monochromated Mo K α radiation (λ = 0.71073 Å) at 296 K. Data reduction included Routine Lorentz and polarization corrections. The multi-scan absorption correction was done using the SADABS program.^[41] The structure was solved using direct methods and refined by the full-matrix least-squares on *F*² with the SHELXS-97 software.^[42] In the final refinement cycles, all the W, As, and Ru atoms were refined

anisotropically, while the O, C and N atoms were refined isotropically. The partial DMA cations and lattice water molecules were located by Fourier map; the remaining DMA cations and lattice water molecules were determined by CHN element analysis and TGA result. The hydrogen atoms of the organic groups were placed in calculated positions and then refined using a riding model. The hydrogen atoms on water molecules were directly included in the molecular formula. Crystallographic data for the structure reported in this paper have been deposited in the Cambridge Crystallographic Data Center with CCDC Number: 1590368. The crystal data and structure refinement parameter are listed in Table 4.

Acknowledgements

We gratefully acknowledge support from the NSFC (21571050) and the Natural Science Foundation of Henan Province.

Keywords: polyoxometalates • ruthenium • arsenotungstate • catalysis • sulfoxidation

- [1] a) H. N. Miras, J. Yan, D.-L. Long, L. Cronin, *Chem. Soc. Rev.* **2012**, *41*, 7403; b) L. Huang, S.-S. Wang, J.-W. Zhao, L. Cheng, G.-Y. Yang, *J. Am. Chem. Soc.* **2014**, *136*, 7637–7642; c) M. Yaqub, S. Imar, F. Laffir, G. Armstrong, T. McCormac, *ACS Appl. Mater. Interfaces* **2015**, *7*, 1046–1056; d) J.-D. Compain, P. Mialane, A. Dolbecq, I. M. Mbomekallé, J. Marrot, F. Sécheresse, E. Rivière, G. Rogez, W. Wernsdorfer, *Angew. Chem.* **2009**, *121*, 3123–3127; e) P. Ma, F. Hu, R. Wan, Y. Huo, D. Zhang, J. Niu, J. Wang, *J. Mater. Chem. C* **2016**, *4*, 5424–5433.
- [2] a) T. Naota, H. Takaya, S.-I. Murahashi, *Chem. Rev.* **1998**, *98*, 2599–2660; b) C. L. Hill, C. M. Prosser-McCarthy, *Coord. Chem. Rev.* **1995**, *143*, 407–455.
- [3] a) P. Putaj, F. Lefebvre, *Coord. Chem. Rev.* **2011**, *255*, 1642–1685; b) N. V. Izarova, M. T. Pope, U. Kortz, *Angew. Chem. Int. Ed.* **2012**, *51*, 9492–9510.
- [4] a) R. Neumann, C. Abu-Gnim, *J. Chem. Soc. Chem. Commun.* **1989**, *18*, 1324–1325; b) M. Higashijima, *Chem. Lett.* **1999**, *28*, 1093–1094; c) K. Yamaguchi, N. Mizuno, *New J. Chem.* **2002**, *26*, 972–974; d) A. M. Khenkin, I. Efremenko, L. Weiner, J. M. L. Martin, R. Neumann, *Chem. Eur. J.* **2010**, *16*, 1356–1364.
- [5] a) A. Bagno, M. Bonchio, A. Sartorel, G. Scorrano, *Eur. J. Inorg. Chem.* **2000**, *2000*, 17–20; b) M. Sadakane, N. Rinn, S. Moroi, H. Kitatomi, T. Ozeki, M. Kurasawa, M. Itakura, S. Hayakawa, K. Kato, M. Miyamoto, S. Ogo, Y. Ide, Z. *Anorg. Allg. Chem.* **2011**, *637*, 1467–1474.
- [6] A. R. Howells, A. Sankarraj, C. Shannon, *J. Am. Chem. Soc.* **2004**, *126*, 12258–12259.
- [7] C. Rong, M. T. Pope, *J. Am. Chem. Soc.* **1992**, *114*, 2932–2938.
- [8] M. Sadakane, D. Tsukuma, M. H. Dickman, B. Bassil, U. Kortz, M. Higashijima, W. Ueda, *Dalton Trans.* **2006**, 4271–4276.
- [9] S. Ogo, M. Miyamoto, Y. Ide, T. Sano, M. Sadakane, *Dalton Trans.* **2012**, *41*, 9901–9907.
- [10] S. Ogo, N. Shimizu, T. Ozeki, Y. Kobayashi, Y. Ide, T. Sano, M. Sadakane, *Dalton Trans.* **2013**, *42*, 2540–2545.
- [11] L.-H. Bi, U. Kortz, B. Keita, L. Nadjo, *Dalton Trans.* **2004**, 3184–3190.
- [12] R. Neumann, A. M. Khenkin, *Inorg. Chem.* **1995**, *34*, 5753–5760.
- [13] M. Sadakane, M. Higashijima, *Dalton Trans.* **2003**, 659–664.
- [14] S.-W. Chen, R. Villanneau, Y. Li, L.-M. Chamoreau, K. Boubekeur, R. Thouvenot, P. Gouzerh, A. Proust, *Eur. J. Inorg. Chem.* **2008**, *2008*, 2137–2142.
- [15] V. Lahootun, C. Besson, R. Villanneau, F. Villain, L.-M. Chamoreau, K. Boubekeur, S. Blanchard, R. Thouvenot, A. Proust, *J. Am. Chem. Soc.* **2007**, *129*, 7127–7135.

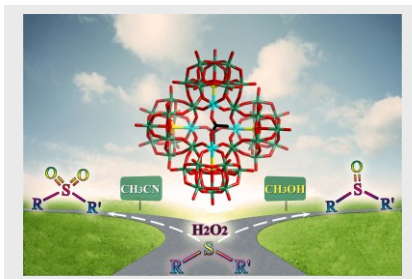
- [16] C. Besson, D. G. Musaev, V. Lahootun, R. Cao, L.-M. Chamoreau, R. Villanneau, F. Villain, R. Thouvenot, Y. V. Geletii, C. L. Hill, et al., *Chem. Eur. J.* **2009**, *15*, 10233–10243.
- [17] V. Artero, D. Laurencin, R. Villanneau, R. Thouvenot, P. Herson, P. Gouzerh, A. Proust, *Inorg. Chem.* **2005**, *44*, 2826–2835.
- [18] J. A. F. Gamelas, H. M. Carapuça, M. S. Balula, D. V. Evtuguin, W. Schlindwein, F. G. Figueiras, V. S. Amaral, A. M. V. Cavaleiro, *Polyhedron* **2010**, *29*, 3066–3073.
- [19] P.-E. Car, M. Guttentag, K. K. Balldridge, R. Alberto, G. R. Patzke, *Green Chem.* **2012**, *14*, 1680–1688.
- [20] I. V. Kalinina, N. V. Izarova, U. Kortz, *Inorg. Chem.* **2012**, *51*, 7442–7444.
- [21] L.-H. Bi, B. Li, S. Bi, L.-X. Wu, *J. Solid State Chem.* **2009**, *182*, 1401–1407.
- [22] L.-H. Bi, G. Al-Kadamany, E. V. Chubarova, M. H. Dickman, L. Chen, D.S. Gopala, R. M. Richards, B. Keita, L. Nadjio, H. Jaensch, G. Mathys, U. Kortz, *Inorg. Chem.* **2009**, *48*, 10068–10077.
- [23] D.-M. Zheng, R.-Q. Wang, Y. Du, G.-F. Hou, L.-X. Wu, L.-H. Bi, *New J. Chem.* **2016**, *40*, 8829–8836.
- [24] F. Robert, M. Leyrie, G. Herve, A. Teze, Y. Jeannin, *Inorg. Chem.* **1980**, *19*, 1746–1752.
- [25] W. Chen, Y. Li, Y. Wang, E. Wang, Z. Su, *Dalton Trans.* **2007**, *38*, 4293–4301.
- [26] U. Kortz, *J. Clust. Sci.* **2003**, *14*, 205–214.
- [27] P. Mialane, A. Dolbecq, E. Rivière, J. Marrot, F. Sécheresse, *Eur. J. Inorg. Chem.* **2004**, *2004*, 33–36.
- [28] J. Niu, K. Wang, H. Chen, J. Zhao, P. Ma, J. Wang, M. Li, Y. Bai, D. Dang, *Cryst. Growth Des.* **2009**, *9*, 4362–4372.
- [29] N. E. Brese, M. O'Keeffe, *Acta Crystallogr. Sect. B* **1991**, *47*, 192–197.
- [30] a) W. J. Randall, T. J. R. Weakley, R. G. Finke, *Inorg. Chem.* **1993**, *32*, 1068–1071; b) S. Ogo, N. Shimizu, T. Ozeki, Y. Kobayashi, Y. Ide, T. Sano, M. Sadakane, *Dalton Trans.* **2013**, *42*, 2540–2545; c) Y. Geletii, B. Botar, P. Kögerler, D. Hillesheim, D. Musaev, C. Hill, *Angew. Chem. Int. Ed.* **2008**, *47*, 3896–3899.
- [31] C. Ritchie, M. Speldrich, R. W. Gable, L. Sorace, P. Kögerler, C. Boskovic, *Inorg. Chem.* **2011**, *50*, 7004–7014.
- [32] P. Ma, R. Wan, Y. Si, F. Hu, Y. Wang, J. Niu, J. Wang, *Dalton Trans.* **2015**, *44*, 11514–11523.
- [33] J.-W. Zhao, C.-M. Wang, J. Zhang, S.-T. Zheng, G.-Y. Yang, *Chem. Eur. J.* **2008**, *14*, 9223–9239.
- [34] Y. Wang, X. Sun, S. Li, P. Ma, J. Wang, J. Niu, *Dalton Trans.* **2015**, *44*, 733–738.
- [35] R. M. Wallace, R. C. Propst, *J. Am. Chem. Soc.* **1969**, *91*, 3779–3785.
- [36] M. C. Carreno, *Chem. Rev.* **1995**, *95*, 1717–1760.
- [37] R. Sheldon, I. W. C. Arends, A. Dijkstra, *Catal. Today* **2000**, *57*, 157–166.
- [38] I. Fernández, N. Khair, *Chem. Rev.* **2003**, *103*, 3651–3706.
- [39] a) E. Baciocchi, M. F. Gerini, A. Lapi, *J. Org. Chem.* **2004**, *69*, 3586–3589; b) S. P. Das, J. J. Boruah, N. Sharma, N. S. Islam, *J. Mol. Catal. Chem.* **2012**, *356*, 36–45; c) S. Doherty, J. G. Knight, M. A. Carroll, J. R. Ellison, S. J. Hobson, S. Stevens, C. Hardacre, P. Goodrich, *Green Chem.* **2015**, *17*, 1559–1571.
- [40] a) A. M. Cojocariu, P. H. Mutin, E. Dumitriu, F. Fajula, A. Vioux, V. Hulea, *Chem. Commun.* **2008**, 5357–5359; b) B. Chen, S. Shang, L. Wang, Y. Zhang, S. Gao, *Chem. Commun.* **2016**, *52*, 481–484.
- [41] G. M. Sheldrick, *SADABS—Bruker AXS area detector scaling and absorption, version 2008/2001*, University of Göttingen: Germany, 2008.
- [42] G. M. Sheldrick, *Acta Crystallogr., Sec. A: Found. Crystallogr.*, **2008**, *64*, 112–122.

Entry for the Table of Contents

FULL PAPER

A crown-shaped Ru-substituted arsenotungstate

$[\text{H}_2\text{N}(\text{CH}_3)_2]_{14}[\text{As}_4\text{W}_{40}\text{O}_{140}\{\text{Ru}_2(\text{CH}_3\text{COO})_2\}_2] \cdot 22\text{H}_2\text{O}$ (**1**), has been prepared by self-assembly strategy. The catalytic activity of **1** towards the selective oxidation of sulfides has been systematically probed.



Mengdan Han, Yanjun Niu, Rong Wan, Qiaofei Xu, Jingkun Lu, Pengtao Ma, Chao Zhang, Jingyang Niu* and Jingping Wang*

Page No. – Page No.

A Crown-Shaped Ru-Substituted Arsenotungstate for Selective Oxidation of Sulfides with Hydrogen Peroxide